yellow $Cp(CO)(PEt_3)FeC_6H_5$. A second yellow band, eluted with 5:1 hexanes/ethyl acetate, was **21**. Solvent was removed in vacuo, and the product oils were redissolved in hexane and cooled to −40 °C. Orange crystalline material was obtained for both products. Yield: 280 mg of **21** (41%); 200 mg of $Cp(CO)(PEt_3)FeC_6H_5$ (32%).

21. ^1H NMR (C_6D_6): δ 0.73 (dt, 9 H, J = 7.5, 15 Hz, P–CH_2CH_3), 1.31 (dq, 3 H, J = 7.5, 22.5 Hz, P–CHH'–), 1.51 (dq, 3 H, J = 7.5, 22.5 Hz, P–CHH'–), 4.30 (s, 5 H, Cp), 7.18 (t, 1 H, J = 7.3 Hz, H(para)), 7.31 (dd, 2 H, J = 7.6, 7.6 Hz, H(meta)), 7.99 (d, 2 H, J = 7.6 Hz, H(ortho)). IR (CH_2Cl_2): ν_{CO} 1912, 1590, 1575, 1550 cm^{-1}. Anal. Calcd $C_{19}H_{25}O_2PFe$: C, 61.31; H, 6.77. Found: C, 60.93; H, 6.91.

Synthesis of $Cp(CO)(PR_3)Fe{=}C(OCH_3)C_6H_5^+OTf^-$ (17, R = Ph; 18, R = Et). General Procedure.[32] (η^5-C_5H_5)(CO)(PR_3)$FeCOC_6H_5$ was dissolved in CH_2Cl_2 and 2 equiv of MeOTf added. After it was stirred at room temperature overnight, the solution turned from clear orange to deep red. The reaction was deemed complete by IR spectroscopy when the acyl (1560 cm^{-1}) and carbonyl (1910 cm^{-1}) absorption bands of the starting benzoyl disappeared and a single absorption band at 1985 cm^{-1} for the heterocarbene grew in. The reaction mixture was filtered through Celite, solvent was removed in vacuo, and the product dark red oil was washed several times with Et_2O.

17. ^1H NMR (CD_2Cl_2): δ 3.39 (s, 3 H, $-OCH_3$), 4.96 (d, 5 H, $^3J_{PH}$ = 1.2 Hz, η^5-C_5H_5), 6.93–8.09 (m, 20 H, $-C_6H_5$'s). ^{13}C NMR (CD_2Cl_2): δ 60.8 ($-OCH_3$), 87.9 (η^5-C_5H_5), 127.2–134.6 (C_6H_5's), 152.0 (C(ipso) of carbene phenyl), 217.0 (d, $^2J_{PC}$ = 28.7 Hz, $-CO$), 333.6 (d, $^2J_{PC}$ = 24.7 Hz, $=C$). IR (CH_2Cl_2): ν_{CO} 1984 cm^{-1}.

18. ^1H NMR (CD_2Cl_2): δ 1.03 (dt, 9 H, J = 7.7, 16.2 Hz, P–CH_2CH_3), 1.85 (m, 6 H, P–CH_2), 3.48 (s, 3 H, $-OCH_3$), 5.09 (d, 5 H, $^3J_{PH}$ = 1.2 Hz, η^5-C_5H_5), 7.44–7.60 (m, 5 H, $-C_6H_5$). ^{13}C NMR (CD_2Cl_2): δ 8.11, P–CH_2CH_3), 21.7 (d, $^1J_{PC}$ = 28.6 Hz, P–CH_2–), 61.3 ($-OCH_3$), 86.8 (η^5-C_5H_5), 133.9, 128.9, 127.2 (C(ortho), C(meta), C-(para)), 152.7 (C(ipso)), 216.5 (d, $^2J_{PC}$ = 28.8 Hz, –CO), 331.6 (d, $^2J_{PC}$ = 21.2 Hz, $=C$). IR (CH_2Cl_2): ν_{CO} 1988 cm^{-1}.

Hydride Addition to $Cp(CO)(PR_3)Fe{=}C(OCH_3)C_6H_5^+$. 17: PR_3 = PPh_3. General Procedure. A 450-μL CD_2Cl_2 solution of **17** (10 mg, 1.9 × 10^{-2} mmol) was prepared in a 5-mm NMR tube at room temperature and added dropwise to 250 μL of a $CD_3OD/CD_3O^-Na^+/NaBH_4$ solution[23] (of the specified $NaBH_4$ concentration) cooled to either 0 or −78 °C, which was purged with nitrogen to facilitate complete and rapid mixing. (All solutions had a 5:1 molar ratio of $NaBH_4$ to $NaOCD_3$.) Upon addition, the deep red color of the heterocarbene discharged immediately to clear orange. When addition was complete, the sample was immediately cooled to −78 °C, sealed under vacuum, and maintained at −78 °C until a ^1H NMR spectrum at −42 °C could be recorded. ^1H NMR showed the product to be pure **4** with no side products. Diastereomer ratios were determined by ^1H NMR integration of the –CH peaks at δ 4.71 for (*SR*)-**4**:(*RS*)-**4** and δ 5.01 for (*SS*)-**4**:(*RR*)-**4** and are summarized in Table IV.

18: PR_3 = PEt_3. General Procedure. A 3-mL CH_2Cl_2 solution of **18** (30 mg, 5.6 × 10^{-2} mmol) was added dropwise to 1 mL of a rapidly stirring $CH_3OH/CH_3O^-Na^+/NaBH_4$ solution (of specified concentration) at 0 °C. (All solutions were 5:1 $NaBH_4/NaOCH_3$.) Immediate discharge of the deep red carbene to clear yellow occurred. A total of 10 mL of CH_2Cl_2 and 10 mL of aqueous bicarbonate was added, the solution stirred rapidly, and the bottom CH_2Cl_2 layer filtered through a plug of Celite/anhydrous K_2CO_3. Solvent was removed in vacuo, yielding 20.2 mg (93%) of red-orange oil. ^1H NMR (C_6D_6) showed the product to be pure **7**. Diastereomer ratios were determined by integration of the –CH peaks at δ 4.91 for (*SR*)-**7**:(*RS*)-**7** and δ 5.30 for (*SS*)-**7**:(*RR*)-**7** and are summarized in Table IV.

Acknowledgment is made to the donors of the Petroleum Research Fund, administered by the American Chemical Society, and to the National Institutes of Health (Grant GM-23938) for the support of this research.

Registry No. **3**, 64494-50-4; [α-*D*]-**3**, 117094-47-0; **4** (isomer 1), 113350-82-6; **4** (isomer 2), 104832-41-9; (*S*)-**5**, 117094-46-9; (*S*)-**6**, 55137-68-3; **7**, 117178-89-9; **7** (isomer 1), 113215-01-3; **7** (isomer 2), 113109-99-2; [α-*D*]-**7** (isomer 1), 117094-48-1; [α-*D*]-**7** (isomer 2), 117178-90-2; **9**, 117180-25-3; **11A**, 113214-96-3; **11S**, 113214-94-1; **12A**, 117178-88-8; **12S**, 117178-92-4; [α-*D*]-**12A**, 117094-51-6; [α-*D*]-**12S**, 117178-94-6; **15** (isomer 1), 117094-49-2; **15** (isomer 2), 117178-91-3; **17**, 117094-55-0; **18**, 117094-57-2; **21**, 117094-53-8; $Cp(CO)_2Fe^-K^+$, 60039-75-0; $Cp(CO)_2FeCOC_6H_5$, 12154-94-8; $Cp(CO)(PPh_3)$-$FeCOC_6H_5$, 12118-59-1; $Cp(CO)(PEt_3)FeC_6H_5$, 117094-52-7.

(32) Cutler, A. R.; Bodnar, T. W. *Synth. React. Inorg. Met.-Org. Chem.* **1985**, *15*(1), 31.

Synthesis, Spectroscopic Characterization, Dynamics, and Phosphine Trapping of $Cp(CO)Fe[\eta^3$-$CH(R)C_6H_5]$ Complexes (R = H, OCH_3)

M. Brookhart,* Robert C. Buck, and Earl Danielson, III

Contribution from the Department of Chemistry, The University of North Carolina at Chapel Hill, Chapel Hill, North Carolina 27599-3290. *Received March 7, 1988*

Abstract: Low-temperature photolysis of $Cp(CO)_2FeCH(R)C_6H_5$ (**1A**, R = H; **1B**, R = OCH_3) yields η^3-benzyl complexes $Cp(CO)Fe(\eta^3$-$CH(R)C_6H_5)$ (**3A**, R = H; **3B**, R = OCH_3), respectively, which have been characterized by ^1H and ^{13}C NMR spectroscopy. The dynamic behavior of **3A** and **3B** has been studied by variable-temperature ^1H NMR spectroscopy. The free energies of activation for the formation of the η^1 species $Cp(CO)Fe(\eta^1$-$CH(R)C_6H_5)$ (**2A**, R = H; **2B**, R = OCH_3) from **3A** and **3B** were determined as 12.0 and 15.4 kcal/mol, respectively. When an excited-state absorption spectrophotometric experiment was used, the η^1 species **2A** could be generated from **1A** and its rate of collapse to **3A** measured as 1 × 10^8 s^{-1} at 293 K. The equilibrium ratio of **3A**:**2A** was estimated as ca. 10^4 at 293 K. Kinetics of trapping of **3A** and **3B** by $P(C_6H_5)_3$ and $P(C_2H_5)_3$ were carried out under pseudo-first-order conditions at low temperatures (202 and 231 K). These data coupled with information from dynamic NMR and flash photolysis studies and, for $P(C_6H_5)_3$, rates of dissociation allow a complete thermodynamic and kinetic description of several of these systems (see free energy diagrams in Figures 4 and 5).

In the preceding paper an investigation of three synthetic routes to chiral-at-iron complexes $Cp(CO)(PR_3)FeCH(OCH_3)C_6H_5$ (R = Ph, Et) was reported.[1] These complexes represent precursors to cationic chiral-at-iron benzylidene complexes, which have been shown to transfer the benzylidene fragment to olefins enantioselectively.[2] One of the routes to these complexes involved the photochemical ligand substitution of $Cp(CO)_2FeCH(OCH_3)C_6H_5$ (**1B**) with PPh_3 and PEt_3. The iron η^3-benzyl complex $Cp(CO)Fe[\eta^3$-$CH(OCH_3)C_6H_5]$ (**3B**) was detected as an interme-

(1) Brookhart, M.; Buck, R. C. *J. Am. Chem. Soc.*, preceding paper in this issue.

(2) (a) Buck, R. C.; Brookhart, M. *Abstracts of Papers*, 191st National Meeting of the American Chemical Society, New York, April 13–18, 1986; American Chemical Society: Washington, DC, 1986; INORG 422. (b) The corresponding chiral-at-iron ethylidene complexes have also been shown to transfer ethylidene to olefins to form cyclopropanes of high enantiomeric purity: Brookhart, M.; Timmers, S.; Tucker, J. R.; Williams, G. D.; Husk, G. R.; Brunner, H.; Hammer, B. *J. Am. Chem. Soc.* **1983**, *105*, 6721.

0002-7863/89/1511-0567$01.50/0

Table I. ^{1}H NMR Data for Complexes **1A**, **3A**, **1B**, and **3B** in Toluene-d_8[a]

complex	T, K	H_A	R	H_o	$H_{o'}$	H_m	$H_{m'}$	H_p	η^5-C_5H_5	ν_{CO}, cm^{-1}
3A (R = H)	225	0.43 (d, J_{gem} = 1.5 Hz)	3.38 (d, J = 1.5 Hz)	2.91 (d, J = 6 Hz)	7.07 (d)	6.55–7.30 (m)			3.41 (s)	1932
	326	1.86 (s)		4.99 (s)						
3B (R = OCH_3)	225	3.21 (s)	3.40 (s)	2.45 (d, J = 6 Hz)	7.85 (d, J = 6 Hz)	7.30–6.60 (m)			3.60 (s)	1925
1A (R = H)	293	2.63 (br s)		6.8–7.5 (m)					3.64 (s)	2000, 1950
1B (R = OCH_3)	293	5.70 (s)	3.16 (s)	7.28 (d, J = 7 Hz)	7.16 (dd, J = 7.7 Hz)		6.93 (dd, J = 7.7 Hz)		4.02 (s)	2010, 1960

[a] All chemical shifts are reported in ppm relative to residual $C_6D_5CD_2H$ at 2.09 ppm. [b] The chemical shift of syn proton $H_{o'}$ is calculated from the average peak at 4.99 ppm (T = 326 K) and the anti H_o peak at 2.91 ppm where average = $(\delta(H_o) + \delta(H_{o'}))/2$.

Table II. ^{13}C NMR Data for Complexes **1A**, **3A**, **1B**, and **3B** in Toluene-d_8[a]

complex	C_1	C_2	C_3	CO	η^5-C_5H_5	C_4, C_7	C_5, C_6	OCH_3
3A (R = H)	23.9	95.1	64.9	223.4	80.4	127.1, 122.6	134.2, 138.2	N/A
3B (R = OCH_3)	53.3	88.8	54.6	223.0	81.59			58.8
1A (R = H)	5.46	153.4		217.8	85.8			N/A
1B (R = OCH_3)	81.1	153.4		217.2, 217.0	86.6			58.9
				obscured by solvent				
				obscured by solvent				
				124.1, 124.6, 128.3 (C_3–C_7)				

[a] All chemical shifts are reported in ppm relative to residual $C_6D_5CD_3$ at 23.8 ppm.

diate in these substitution reactions. Furthermore, **3B** was implicated as a key intermediate in the racemization of the chiral carbon center adjacent to iron in optically active (*R*)-**1B** during the photochemical reaction.

While η^3-allyl complexes are common,[3] relatively few analogous η^3-benzyl (η^3-$CH_2C_6H_5$) species have been reported. King[4] reported the first η^3-benzyl complex $Cp(CO)_2Mo(\eta^3$-$CH_2C_6H_5)$. Cotton[5a,b] reported a detailed dynamic NMR study of the mechanism of fluxionality of derivatives of $Cp(CO)_2Mo(\eta^3$-$CH_2C_6H_5)$ while recently Mann[5c] has studied ring-methylated derivatives and offered a reinterpretation of the mechanism of fluxionality of these molybdenum η^3-benzyl complexes. Other η^3-benzyl derivatives of W,[5a,b,11,16] Fe,[14] Ru,[15] Co,[9] Pd,[7,8,10,12] Rh,[6,13] Ir,[6] Pt,[6,12] and Ni[8,17] have been described. Recently, Wrighton[18] reported spectroscopic evidence for the first iron η^3-benzyl complexes $(\eta^5$-$C_5H_5)(CO)Fe(\eta^3$-$CH_2C_6H_5)$ (**3A**) and $(\eta^5$-$C_5Me_5)$-$(CO)Fe(\eta^3$-$CH_2C_6H_5)$ as products arising from −77 °C (196 K) photochemical decarbonylation of the corresponding dicarbonyl complexes. Wrighton also reported that the η^3-benzyl complexes were rapidly trapped by CO and PPh_3 at 298 K to form $(\eta^5$-$C_5R_5)(CO)(L)Fe(\eta^1$-$CH_2C_6H_5)$(R = H, Me; L = PPh_3, CO).

This paper describes a detailed variable-temperature ^{1}H NMR analysis of the fluxional processes of $Cp(CO)Fe(\eta^3$-$CH_2C_6H_5)$ (**3A**) and $Cp(CO)Fe[\eta^3$-$CH(OCH_3)C_6H_5]$ (**3B**) and their rates of trapping with PPh_3 and PEt_3. In addition, we report results of an excited-state absorption kinetic spectrophotometric experiment to determine the barrier for collapse of the 16e $Cp(CO)$-$Fe(\eta^1$-$CH_2C_6H_5)$ (**2A**) to the 18e η^3-benzyl complex **3A**. These results allow the formulation of a complete kinetic and thermodynamic picture of the dynamics of **3A** and trapping of **3A** with PPh_3 as well as a thermodynamic and kinetic description of the formation of and PPh_3 dissociation from the *SR*:*RS* and *SS*:*RR* diastereomers of $Cp(CO)(PPh_3)FeCH(OCH_3)C_6H_5$. This work fully supports and complements the synthetic observations and mechanistic analysis detailed in the previous paper.[1]

Results and Discussion

A. Synthesis and Spectral Characterization of η^3-Benzyl Complexes. Photolysis of a clear yellow toluene solution of $Cp(CO)_2FeCH(R')C_6H_5$ (**1A**, R′ = H; **1B**, R′ = OCH_3) at −80 °C induces rapid CO loss to form deep red solutions. The product formed from the collapse of the 16e intermediate $[Cp(CO)Fe(\eta^1$-$CH(R')C_6H_5)]$ **2** is the 18e iron η^3-benzyl complex $Cp(CO)Fe[\eta^3$-$CH(R')C_6H_5]$ **3** (eq 1). η^3-Benzyl complexes **3A** and

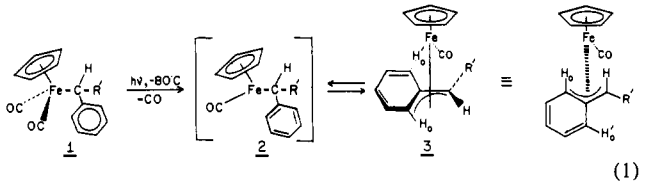

(1)

3B were characterized by ^{1}H NMR, ^{13}C NMR, and IR spectroscopy. Both **3A** and **3B** were sufficiently stable in solution in a sealed NMR tube to record NMR spectra up to 323 K. Warming at 1–2 h at 293 K or above resulted in decomposition of both complexes, with **3B** being less stable. Spectroscopic data for **3A** and **3B** and that of their precursor dicarbonyl complexes **1A** and **1B** are summarized in Tables I and II. Peak assignments were made on the basis of comparisons with known compounds and ^{1}H NMR decoupling experiments.

The ^{1}H NMR chemical shifts of the benzylic hydrogens (225 K) of **3A** appear as two distinct doublets (J_{gem} = 1.5 Hz) at 0.43 ppm (H_A) and 3.38 ppm (H_S) for the inequivalent anti and syn benzylic hydrogens of **3A**.[19] Similarly, the ortho hydrogens of

(3) (a) Clarke, H. L. *J. Organomet. Chem.* **1974**, *80*, 155. (b) King, R. B. In *The Organic Chemistry of Iron*; Von Gustorf, E. A. K., Grevels, F.-W., Fischler, I., Eds.; Academic: New York, 1978; Vol. 1, pp 463–523. (c) Deeming, A. J. In *Comprehensive Organometallic Chemistry*; Wilkinson, G., Stone, F. G. A., Abel, E. W., Eds.; Pergamon: New York, 1982; Vol. 4, 31.3.2, pp 399–423.
(4) King, R. B., Fronzaglia, A. *J. Am. Chem. Soc.* **1966**, *88*, 709.
(5) (a) Cotton, F. A.; Marks, T. J. *J. Am. Chem. Soc.* **1969**, *91*, 1339. (b) Cotton, F. A.; La Prade, M. D. *Ibid.* **1968**, *90*, 5418. (c) Mann, B. E.; Shaw, J. P. *J. Organomet. Chem.* **1987**, *326*, C13.
(6) O'Connor, G. J. *Inorg. Nucl. Chem.* **1970**, *32*, 2299.
(7) Stevens, R. R., Shier, G. D. *J. Organomet. Chem.* **1970**, *21*, 495.
(8) (a) Stille, J. K., Fries, R. W. *Synth. React. Inorg. Met.-Org. Chem.* **1971**, *1*, 295. (b) Stille, J. K., Becker, Y. *J. Am. Chem. Soc.* **1978**, *100*, 845.
(9) (a) Muetterties, E. L. *J. Am. Chem. Soc.* **1974**, *96*, 7920. (b) Pälyi, G., Galamb, V. *J. Chem. Soc., Chem. Commun.* **1982**, 487.
(10) Klabunde, K. J., Roberts, J. S. *J. Organomet. Chem.* **1977**, *99*, 2509.
(11) (a) Wojcicki, A.; Severson, R. G. *J. Organomet. Chem.* **1978**, *157*, 173. (b) Wojcicki, A., Shiu-Chin, H. S. *Organometallics* **1983**, *2*, 1296.
(12) Maitlis, P. M.; Mann, B. E.; Keasey, A.; Sonoda, A. *J. Chem. Soc., Dalton Trans.* **1979**, 338.
(13) Stühle, H.-O. *Angew. Chem., Int. Ed. Engl.* **1980**, *19*, 468.
(14) Chen, J.; Lei, G.; Xu, W.; Pan, Z.; Zhang, S.; Zhang, Z.; Jin, X.; Shao, M.; Tang, Y. *Organometallics* **1987**, *12*, 2461.
(15) Bennett, M. A.; McMahon, I. J.; Turney, T. W. *Angew. Chem. Int. Ed. Engl.* **1982**, *21*, 379.
(16) Stone, F. G. A.; Jeffery, J. C.; Laurie, J. C. V.; Moore, I. *J. Organomet. Chem.* **1983**, *258*, C37.
(17) Carmona, E.; Marin, J. M.; Daneque, M.; Poveda, M. L. *Organometallics* **1987**, *6*, 1757.
(18) Wrighton, M. S.; Blaha, J. P. *J. Am. Chem. Soc.* **1985**, *107*, 2694.

(19) The terminology is the same used for η^3-allyl species. Substituents at the terminal carbons on the η^3-fragment are designated anti or syn with respect to the substituent bound to the central carbon of the η^3-fragment.[3]

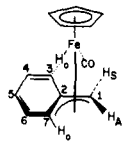

3A

the phenyl ring H_o and H_o' have very different environments in **3A** with chemical shifts of 2.91 ppm (H_o) and 7.07 ppm (H_o').[20] An upfield shift of the ^{13}C NMR signals of C_1, C_2, and η^5-C_5H_5 and a downfield shift of CO also occur upon conversion to **3A**. The most distinct change occurs for C_2 and C_3 as they become part of the η^3-benzyl fragment. Their chemical shifts change from 153.4 and 125 ppm in **1A** to 95.1 and 64.9 ppm in **3A**, respectively. Finally, the carbonyl stretching frequency shifts from 2000 and 1960 cm^{-1} for **1A** to 1932 cm^{-1} for **3A**.

The spectral changes observed for conversion of **1B** to **3B** are similar to those noted for conversion of **1A** to **3A** with one important exception. *Complex* **3B** *can exist as two isomers, with* the benzylic hydrogen H_A occupying either the anti (**3B**) or syn (**3B'**) site[19] (eq 2). On the basis of the data for **3A**, hydrogens

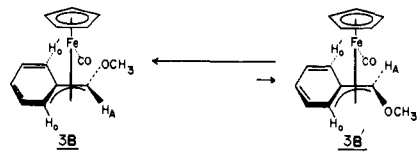

3B 3B' (2)

in these two sites should have very different chemical shifts. Only one signal for H_A is observed in the ^1H NMR spectrum of **3B** at 3.21 ppm, which indicates that **3B** exists as primarily one isomer (>98%). The chemical shift of H_A is at higher field than the syn hydrogen H_S of **3A** (3.38 ppm) despite the electron-withdrawing effect of the geminal methoxy group. If H_A were syn as in **3B**, its chemical shift would be much lower than the analogous syn hydrogen of **3A**. Thus, the upfield shift of H_A (3.21 ppm) clearly indicates that it must be exclusively anti, with the $-OCH_3$ group occupying the syn position as would be sterically preferred (eq 2). This structural limitation for **3B** is critical when considering the fluxional processes that **3B** may undergo in comparison to **3A** (see below).

B. Dynamics of η^3-Benzyl Complexes 3A and 3B. The fluxional processes of **3A** and **3B** were studied by variable-temperature ^1H NMR spectroscopy at 200 MHz. As a sealed sample of **3A** in toluene-d_8 is slowly warmed from −82 °C, a number of spectral changes are observed. The signals for the benzylic hydrogens, H_A and H_S, at 0.43 and 3.38 ppm and the ortho hydrogens, H_o and $H_{o'}$, at 2.91 and 7.07 ppm broaden at the same initial rate, disappear into the base line at 270 K, and then reappear as broad singlets at 1.86 and 4.99 ppm, respectively, at 315 K. Due to the large chemical shift difference for these pairs of signals (i.e. 590 Hz for H_A and H_S; 838 Hz for H_o and $H_{o'}$), their coalescence temperatures T_c are not sharply defined. Their rates of site exchange are the same within experimental error as measured by the slow exchange, fast exchange, and coalescence approximations (see Table III).

The scrambling process is best explained by σ, π interconversions and inversion at iron as shown in Figure 1.[21,22] The π-benzyl

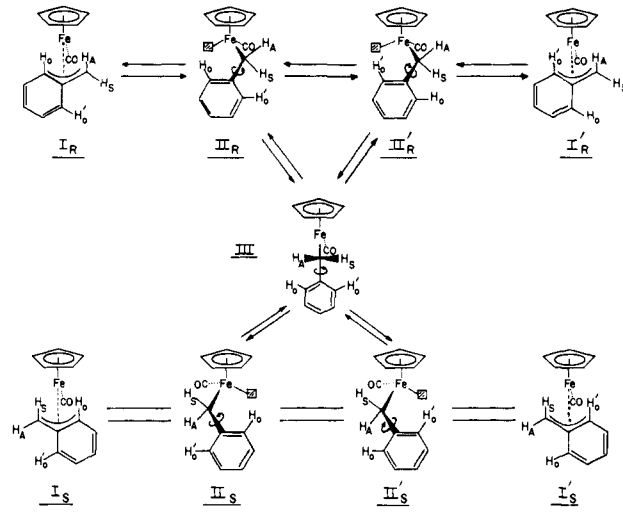

Figure 1.

complex is assumed to have the geometry shown in I with the "benzo" group trans to cyclopentadienyl in the endo conformation.[23] The metal center in I is chiral, and we shall arbitrarily begin an analysis of the system with the (*R*) enantiomer (priorities: Cp > η^2-phenyl > CO > η^1-CH_2). Dechelation of the benzo group from I_R initially generates the 16e species II_R in which Cα is sp^3 hybridized and the iron center retains chirality (octahedral geometry, one vacant coordination site). Collapse of II_R regenerates I_R. Rotation about the Cα–C(ipso) bond interconverts H_o and $H_{o'}$ ($II_R \rightleftharpoons II_{R'}$). Collapse after aryl rotation generates $I_{R'}$. To interconvert H_A and H_S, inversion of the iron center in the σ-complex must occur via III.[24] Species III possesses a plane of symmetry with $H_A \equiv H_B$. (Although this species could be the most stable form of the σ-complex, it is more likely a low-lying transition state connecting I_R and I_S.)[24] Upon collapse of III, with inversion at iron to generate I_S, site exchange of H_A and H_S is achieved. The fact that the rates of site exchange for H_A, H_S and H_o, $H_{o'}$ are nearly the same implies that when the σ-complex II is formed, its lifetime is sufficient to allow both aryl rotation and iron inversion to occur before collapse. (A situation where, for example, $H_o \rightleftharpoons H_{o'}$ was faster than $H_A \rightleftharpoons H_S$ could have obtained if aryl rotation and collapse in II was faster than inversion, but apparently this is not the case.)

In the case of **3B**, only one isomer (>98% H_A anti) is present. The only fluxional process observed is averaging of the H_o and $H_{o'}$ protons, which must occur via aryl rotation. As a sample of **3B** in toluene-d_8 is slowly warmed from −71 °C, the signals for H_o and $H_{o'}$ at 2.45 and 7.85 ppm slowly broaden and coalesce at 323 K (+50 °C). The rate of exchange was measured by the slow-exchange approximation[22] to be k(**3B**,**2B**) = 22 s^{-1} (T = 293 K), giving $\Delta G^{\ddagger}$(ortho) = 15.4 kcal/mol. The signal at 3.21 ppm for H_A remains sharp over the temperatures examined (−71 to +50 °C) with no significant line broadening (<2 Hz) or change in chemical shift (<0.05 ppm). In addition, no minor syn isomer is detected at low temperatures. No information is obtained regarding iron inversion (no intermediate with a plane of symmetry can be achieved), and the process illustrated in eq 3 is sufficient to explain the observed dynamic behavior.[21]

The configuration at the chiral Cα carbon of **3B** cannot be inverted by this process. Inversion of configuration can *only* occur by bond breaking–remaking processes, experimental evidence and

(20) Wrighton[18] has reported the following for **3A**. ^1H NMR (methylcyclohexane-d_{14}, T = 196 K): δ 7.0 (s, 5 H), 4.41 (s, 5 H), 3.59 (br s, 2 H). However, we find two distinct resonances for both the benzylic and ortho hydrogens at 225 K as shown in Table I.

(21) As discussed by Mann[5c] for Mo derivatives, a mechanism involving 1,5 iron migration coupled with allyl rotation could account for the dynamic behavior of **3A** without involving η^1-intermediates. However, for the methoxy derivative, **3B**, such a mechanism is not consistent with the fluxional behavior and η^1-derivatives must be involved. Since the activation barriers for fluxional behavior of **3A** and **3B** are so similar, we conclude that the η^1-mechanism shown in Figure 1 is the most reasonable one to propose for both **3A** and **3B**.

(22) Although the $\Delta G^{\ddagger}$ values in Table III have substantial error limits, the trend is clearly toward decreasing values of $\Delta G^{\ddagger}$ with increasing temperature. This suggests a positive $\Delta S^{\ddagger}$, which is consistent with the $\eta^3 \rightarrow \eta^1$ conversion.

(23) The endo conformation[3] (η^3 in a "V") where the benzo group is trans to cyclopentadiene should be more sterically favorable than the exo conformation (η^3 in a "Λ") where the benzo group is cis to cyclopentadiene, a more sterically crowded conformation. An X-ray crystallographic study by Cotton[5b] shows that this is in fact the case for the solid-state structure of Cp-$(CO)_2Mo(\eta^3\text{-}CH_2\text{-}p\text{-}CH_3C_6H_4)$.

(24) The pyramidal conformation has been shown to be of lower energy than the planar conformation for the $Cp(CO)_2Mn$ 16e fragment. In addition, the barrier for inversion at manganese is quite low (i.e. <5 kcal/mol): Hofmann, P. *Angew. Chem. Int. Ed. Engl.* **1977**, *16*, 536.

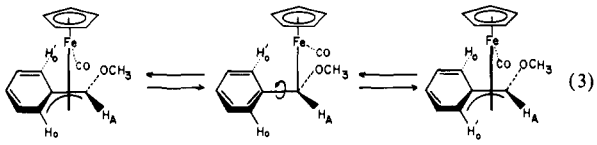

(3)

a proposed mechanism for which have been outlined in the previous paper.[1] In further support of this conclusion, Stille[8b] has shown that (*S*)-(−)-*trans*-chloro(η^1-α-deuteriobenzyl)bis(triethylphosphine)palladium(II) (**6**) when treated with sodium tetraphenylborate gives (*S*)-(+)-(η^3-α-deuteriobenzyl)bis(triethylphosphine)palladium(II) tetraphenylborate (**7**), which retains optical activity in solution and, when treated with lithium chloride, reforms **6** with 94% net retention of configuration at the benzyl carbon (eq 4). Similarly, chirality retention at methylene has been observed in substituted π-allyl palladium complexes.[25]

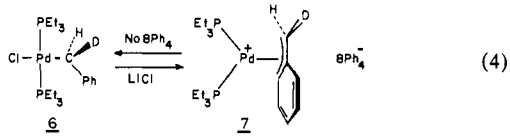

(4)

Excited-state absorption spectroscopy was performed in an attempt to detect **2A** and measure its rate of collapse to **3A**. Wrighton[18] has reported the 196 K UV/vis spectrum of **1A** and **3A**. η^3-Benzyl complex **3A** was shown to have a distinct weak absorption at 460 nm, well removed from the strong absorption bands of **1A**. The solution UV/vis spectrum of **1A** shows strong bands at λ_{max} = 222 and 318 nm with weak tailing but nonzero absorption at 460 nm. (The UV/vis spectrum is contained in the supplementary material.) On the basis of these observations, the barrier to collapse of the 16e unsaturated complex **2A** to **3A** could be determined by irradiating a solution of **1A** and then monitoring by UV/vis spectroscopy the appearance of the 460-nm absorption band of **3A**.

Rigorously degassed samples of a 1.3 × 10^{-4} M solution of **1A** in *n*-hexane were irradiated with 355-nm pulses of laser light while the absorbance of the solution at 460 nm was monitored. The plot of the change in absorbance (ΔA) of the solution at 460 nm versus time is shown in Figure 2a. Analysis of the data in Figure 2a shows a weak irresolvably fast bleaching of the ground-state absorbance (0–4 ns) followed by a first-order increase in absorption (4–30 ns) and finally a slow second-order decrease in absorption, which eventually returns to the base line. These observations are consistent with the mechanism shown in eq 5. The first, very

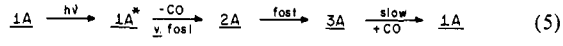

(5)

fast, bleaching process is interpreted as loss of CO from excited **1A*** to form **2A**. The second process is the rapid, first-order collapse of **2A** to **3A**. Kinetic analysis of this growth is depicted in Figure 2b. From a least-squares fit, a first-order rate constant of 1.04 (±0.06) × 10^8 s^{-1} was determined. The third process is the slow, second-order recombination of **3A** with CO to regenerate **1A**.[26] This mechanistic interpretation is supported by the observation that the spectrum of an aliquot of the starting solution of **1A** is essentially identical within experimental error to the spectrum of an irradiated sample that was allowed to stand in the dark for 24 h. This clearly demonstrates that the product(s) formed from photolysis of **1A** under these conditions return to **1A** and little if any M–CH_2Ph bond scission occurs. (Upon prolonged irradiation of solutions of **1A**, Wrighton[18] observed products resulting from iron–carbon bond scission and radical

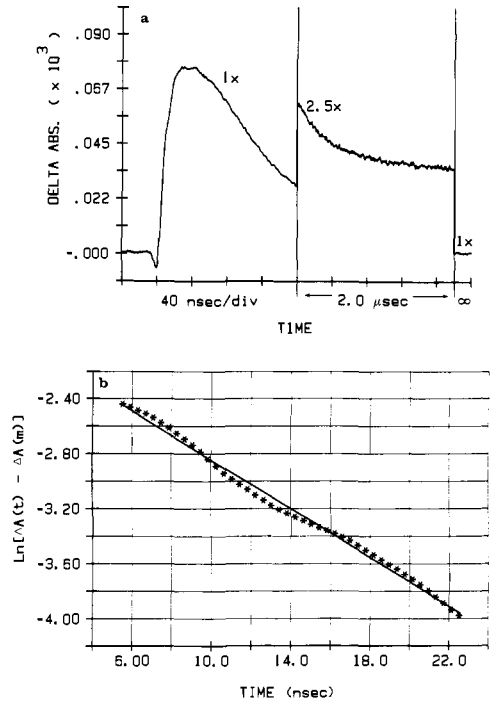

Figure 2. (a) Excited-state absorbance resulting from 355 nm. Excitation of $(Cp)(CO)_2Fe(\eta^1\text{-}CH_2C_6H_5)$ (1.3 × 10^{-4} N in *n*-hexane) as monitored at 460 nm. The axes are arbitrarily scaled for clarity. (b) First-order kinetic plot for the growth of absorbance observed in Figure I at 460 nm (k_{obs} = 1.04 (±0.06) × 10^8 s^{-1}).

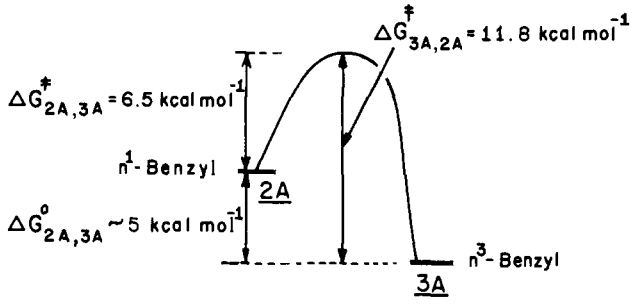

Figure 3.

intermediates.) Irradiation of a much more concentrated solution of **1A** under these same reaction conditions rapidly generated brownish insoluble solid in the reaction solution. No insoluble decomposition products were observed after irradiation of the 1.3 × 10^{-4} M solution of **1A**.

If the proposed mechanism is correct, the barrier to collapse of **2A** to **3A**, $\Delta G^{\ddagger}$(**2A**,**3A**), is approximately 6.5 kcal/mol (k = 10^8 s^{-1}, T = 293 K), and a free energy diagram describing the interconversion of **3A** and **2A** can be constructed (Figure 3). The barrier for conversion of **3A** to **2A**, $\Delta G^{\ddagger}$(**3A**,**2A**), is 11.8 kcal/mol as determined by variable-temperature ^{1}H NMR (see above). On the basis of this data, the ground-state energy difference ΔG°(**2A**,**3A**) between **2A** and **3A** is approximately 5 kcal/mol, which translates into an equilibrium constant K_{eq} of ca. 10^4 (293 °C).

C. Phosphine Trapping Reactions. Complexes **3A** and **3B** are readily trapped with phosphine ligands PR_3 to form complexes $Cp(CO)(PR_3)FeCH(R')C_6H_5$ (eq 6). In a typical experiment,

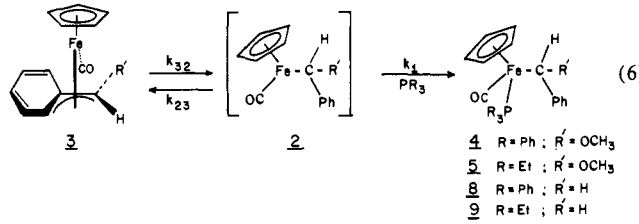

(6)

4 R = Ph ; R′ = OCH_3
5 R = Et ; R′ = OCH_3
8 R = Ph ; R′ = H
9 R = Et ; R′ = H

(25) (a) Vrieze, A. K.; Van Leeuwen, P. W. N. M. *Prog. Inorg. Chem.* **1971**, *14*, 1. (b) Faller, J. W.; Thimsen, M. E., Mattina, M. J. *J. Am. Chem. Soc.* **1971**, *93*, 2642. (c) Faller, J. W.; Tulley, M. T. *Ibid.* **1972**, *94*, 2676.

(26) Good equal-concentration, second-order kinetics were observed for the decay from near the peak maximum out to ca. 1300 ns (k = 1.3 × $10^9/\Delta\epsilon$ M^{-1} s^{-1}). Beyond this time, kinetics exhibit negative curvature in a second-order plot. The low signal/noise level at long times precludes accurate analysis; however, base-line recovery was complete. Kinetics at long times will be complicated by diffusion of CO from the solution.

Table III. Rates of Site Exchange for Benzylic and Ortho Protons of η^3-Benzyl Complex **3A**

method	H_A, H_S exchange		H_o, $H_{o'}$ exchange		
	k, s^{-1}	$\Delta G^{\ddagger}$ kcal/mol	k, s^{-1}	$\Delta G^{\ddagger}$, kcal/mol	T, K
slow-exchange approximation	119	12.6 ± 0.2	113	12.6 ± 0.2	258
coalescence	1.3×10^3	11.9 ± 0.4	1.9×10^3	12.2 ± 0.4	
fast-exchange approximation	5.8×10^4	11.6 ± 0.4	4.1×10^4	11.8 ± 0.4	315

Table IV. $Cp(CO)(PR_3)FeCH(R')C_6H_5$ Products from PR_3 Trapping of η^3-Benzyls **3A** and **3B** with ^1H NMR Data (Toluene-d_8)[a]

	R′	R		δ(H_A)	δ(R′)	δ(η⁵-C₅H₅)	diast ratio *SR*:*RS* to *SS*:*RR*
3B	OCH_3	Ph	(*SR*)-**4**:(*RS*)-**4** (major)	5.17 (d), J_{PH} = 9.2 Hz	2.83 (s)	4.10 (s)	2:1
			(*SS*)-**4**:(*RS*)-**4** (minor)	5.32 (d), J_{PH} = 6.9 Hz	2.30 (s)	3.83 (s)	
3B	OCH_3	Et	(*RS*)-**5**:(*SR*)-**5** (major)	4.93 (d), J_{PH} = 8.9 Hz	3.18 (s)	4.07 (d), J_{PH} = 0.9 Hz	3:2
			(*SS*)-**5**:(*RR*)-**5** (minor)	5.19 (d), J_{PH} = 6.9 Hz	3.07 (s)	3.78 (s)	
3A	H	Ph	**8**	2.18 (dd), J = 10.5, 8 Hz	2.70 (dd), J = 8, 4 Hz	3.96 (s)	N/A
3A	H	Et	**9**	1.70 (dd), J = 8, 8 Hz	2.21 (dd), J = 8, 5 Hz	3.95 (s)	N/A

[a] All chemical shifts are in ppm relative to δ 2.09 for toluene-d_8.

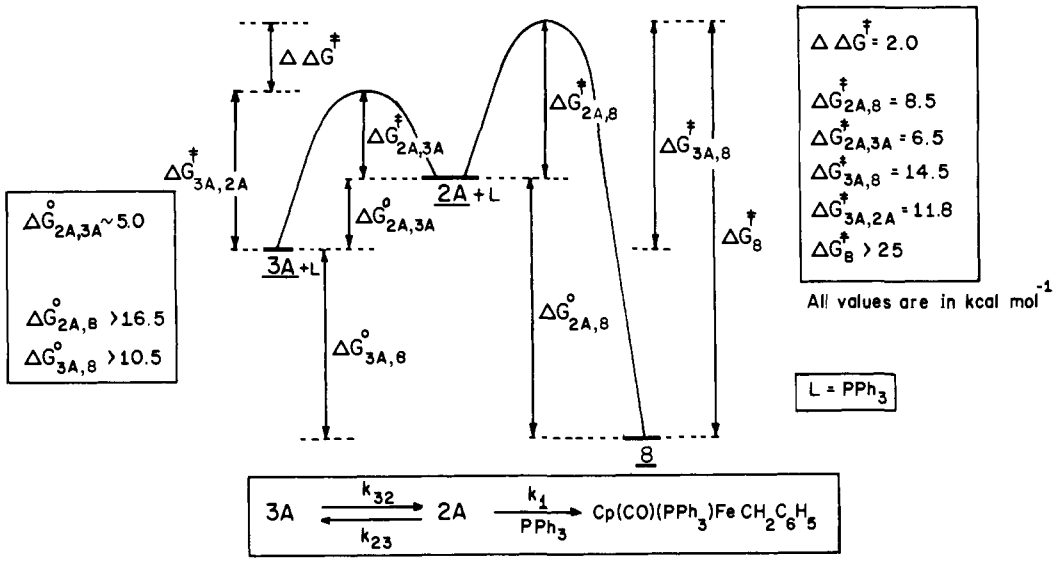

Figure 4.

6 equiv of phosphine were dissolved in 110 μL of toluene-d_8 and added to a deep red −80 °C solution of either **3A** or **3B**. The samples were placed in the NMR probe at −78 °C and slowly warmed. The deep red η^3-benzyl solution discharges to clear yellow-orange upon phosphine trapping. Complex **3A** was trapped completely by PEt_3 before a spectrum could be recorded (−80 °C) while the onset of PPh_3 trapping began at −71 °C. Complex **3B** is trapped by PPh_3 and PEt_3 with the onset of trapping at approximately −50 °C. Although overall diastereoselection is low, the major product formed in all cases was the enantiomeric pair with $Fe_SC\alpha_R$ and $Fe_RC\alpha_S$ configurations.[27] The ^1H NMR spectroscopic data for the products of phosphine trapping is given in Table IV.

Kinetics of PPh_3 and PEt_3 trapping of **3A** and **3B** are summarized in Table V. Rates were determined by adding a 220-μL toluene-d_8 solution (containing the indicated number of equivalents of phosphine relative to η^3-benzyl) to a −80 °C (for **3B**) or −90 °C (for **3A**) toluene-d_8 solution of the η^3-benzyl complex. The rates were determined by ^1H NMR spectroscopy, measuring the decrease in the integral of the η^3-benzyl complex over time versus residual $C_6D_5CD_2H$, which was used as an internal reference. The trapping reaction follows pseudo-first-order kinetics. The slope of the plot of −ln [η^3-benzyl] versus time (seconds) yields k_{obs}, which is the product of the true second-order rate constant k_1 and phosphine concentration:

$$\frac{d[\eta^3\text{-benzyl}]}{dt} = k_1[PR_3][\eta^3\text{-benzyl}]$$

$$k_{obs} = k_1[PR_3]$$

The second-order rate [k(**3A**,**8**)] of PPh_3 trapping of **3A** to form $Cp(CO)(PPh_3)FeCH_2C_6H_5$ (**8**) along with the results from the excited-state absorption experiment to determine the barrier to collapse of **2A** to **3A** allows the construction of a free energy diagram, which gives a full kinetic and thermodynamic description of the trapping of **3A** with PPh_3 (Figure 4). The barrier to trapping **2A** with PPh_3, $\Delta G^{\ddagger}$(**2A**,**8**), of 8.5 kcal/mol is equal to the difference between the barrier to PPh_3 trapping of **3A**, $\Delta G^{\ddagger}$(**3A**,**8**) (from Table V), and the ground-state energy difference between **3A** and **2A**, ΔG°(**2A**,**3A**). Thus, $\Delta G^{\ddagger}$(**2A**,**8**) is approximately 2 kcal/mol greater than $\Delta G^{\ddagger}$(**2A**,**3A**), meaning that the rate of recollapse of **2A** to **3A** is approximately 30 times faster than PPh_3 trapping of **2A** at 293 K at I M PPh_3 (k(**2A**,**8**) = 2.6 × 10^6 s^{-1} L mol^{-1}, k(**2A**,**3A**) = 10^8 s^{-1}). In addition, no evidence of PPh_3 dissociation from **8** was observed when 8 equiv of PEt_3 were added to a solution of **8**, and the sample was monitored for 72 h. This indicates a substantial barrier to PPh_3 dissociation from **8**. If a *minimum* half-life of 144 h at 293 K is assumed, the barrier to PPh_3 dissociation from **8** $\Delta G^{\ddagger}$(**8**) has a minimum value of 25

(27) See preceding paper[1] for a discussion of the configurational assignment of the diastereomers of **4** and **5**.

Table V. Rates of Phosphine Trapping of η^3-Benzyl Complexes 3A and 3B

η^3-benzyl	PR_3	equiv of PR_3	T, K	k_{obs}, s^{-1}	t, min	k_1[a]	$\Delta G^{\ddagger}$,[b] kcal/mol
3B	PEt_3	6.5	231	7.20×10^{-4}	11.2	2.40×10^{-3}	16.2
	PEt_3	10	231	1.22×10^{-3}	9.5	2.65×10^{-3}	16.1
	PEt_3	15	231	1.97×10^{-3}	5.9	2.81×10^{-3}	16.1
	PPh_3	5	231	4.5×10^{-4}	25.7	1.96×10^{-3}	16.3
	PPh_3	10	231	1.05×10^{-3}	11.0	2.28×10^{-3}	16.2
3A	PPh_3	6.8	202	3.0×10^{-4}	38.5	8.5×10^{-4}	14.5
	PEt_3	6.8	202		<seconds		

[a] $k_1 = k_{obs}/[PR_3]$ in units of s^{-1} L mol^{-1}. [b] $\Delta G^{\ddagger}$ is calculated from k_1.

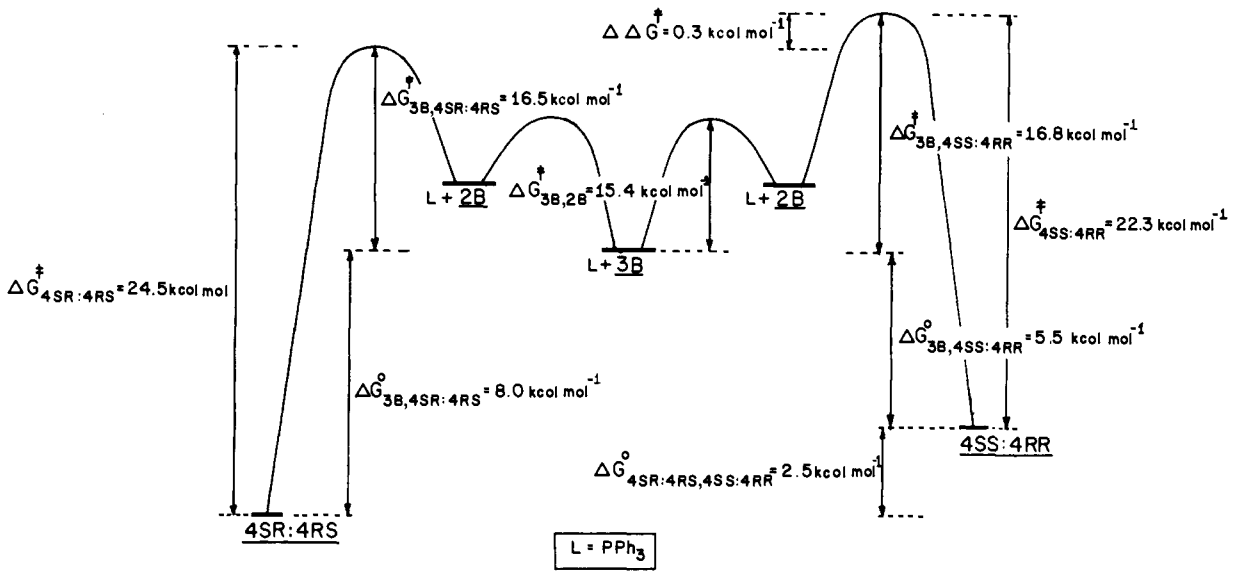

Figure 5.

kcal/mol. This sets a minimum value of 10.5 kcal/mol for the ground-state energy difference between **8** and **3A** plus PPh_3 [ΔG°(**3A**,**8**)].

The second-order rate [k(**3B**,**4**)] of PPh_3 trapping of **3B** (see Table V) coupled with earlier results presented herein and in the preceding paper[1] allow the construction of a free energy diagram, which gives a kinetic and thermodynamic description of the formation of and PPh_3 dissociation from the (*SR*)-**4**:(*RS*)-**4** and (*SS*)-**4**:(*RR*)-**4** diastereomers of $Cp(CO)(PPh_3)FeCH(OCH_3)C_6H_5$ (Figure 5). Since the barrier to collapse of **2B** to **3B** is not known, $\Delta G^{\ddagger}$(**2B**,**3B**) and ΔG°(**2B**,**3B**) could not be determined.[28] When the *overall* rate of trapping of **3B** with PR_3 (Table V) together with the product ratios (*SR*)-**4**:(*RS*)-**4** to (*SS*)-**4**:(*RR*)-**4** is used, the individual trapping rates are calculated to be k(**3B**,(*SR*)-**4**:(*RS*)-**4**) = 1.3×10^{-3} s^{-1} L mol^{-1} ($\Delta G^{\ddagger}$(**3B**,(*SR*)-**4**:(*RS*)-**4**) = 16.5 kcal/mol) and k(**3B**,(*SS*)-**4**:(*RR*)-**4**) = 6.7×10^{-4} s^{-1} L mol^{-1} ($\Delta G^{\ddagger}$(**3B**,(*SS*)-**4**:(*RR*)-**4**) = 18.8 kcal/mol) at 231 K. This corresponds to a $\Delta\Delta G^{\ddagger}$ = 0.3 kcal/mol (see Figure 5), which agrees well with the value calculated independently from the barriers to PPh_3 dissociation, $\Delta G^{\ddagger}$((*SR*)-**4**:(*RS*)-**4**) and $\Delta G^{\ddagger}$((*SS*)-**4**:(*RR*)-**4**), coupled with the ground-state energy difference between (*SR*)-**4**:(*RS*)-**4** and (*SS*)-**4**:(*RR*)-**4**, ΔG°((*SR*)-**4**:(*RS*)-**4**,(*SS*)-**4**:(*RR*)-**4**) determined in the previous paper.[1]

The ground-state energy differences ΔG°(**3B**,(*SR*)-**4**:(*RS*)-**4**) and ΔG°(**3B**,(*SS*)-**4**:(*RR*)-**4**) are 8 and 5.5 kcal/mol as calculated from the difference between the barrier to PPh_3 dissociation and the barrier to PPh_3 trapping of **3B** (i.e. ΔG°(**3B**,(*SR*)-**4**:(*RS*)-**4**) = $\Delta G^{\ddagger}$((*SR*)-**4**:(*RS*)-**4**) − $\Delta G^{\ddagger}$(**3B**,(*SR*)-**4**:(*RS*)-**4**)). These ground-state energy diferences are smaller than the >10.5 kcal/mol ΔG°(**3A**,**8**) ground-state energy difference between **3A** and **8**. This result is expected since PPh_3 readily dissociates from **4** but not from **8**.

(28) The barrier to collapse of **2A** to **3A**, $\Delta G^{\ddagger}$(**2A**,**3A**), is *not* a good estimate of the barrier to collapse of **2B** to **3B**. If this were the case, calculations would give ΔG°(**2B**,**3B**) = 9 kcal/mol and the barriers to trapping **2B** with PPh_3 $\Delta G^{\ddagger}$(**2B**,(*SR*)-**4**:(*RS*)-**4**) and $\Delta G^{\ddagger}$(**2B**,(*SS*)-**4**:(*RR*)-**4**) of 7.5 and 7.8 kcal/mol, respectively, meaning that PPh_3 trapping of **2B** was *faster* than PPh_3 trapping of **2A**. This seems unlikely since it is clear that **3A** to **2A** conversion is much more facile than **3B** to **2B** ($\Delta G^{\ddagger}$(**3A**,**2A**) < $\Delta G^{\ddagger}$(**3B**,**2B**)). Also, PPh_3 readily dissociates from complexes **4** but not **8**. These observations indicate that the ground-state energy difference between **2B** and **3B**, ΔG°(**2B**,**3B**), must be greater than 9 kcal/mol and collapse of **2B** to **3B** *faster* than collapse of **2A** to **3A**.

Summary

The iron η^3-benzyl complexes $Cp(CO)Fe(\eta^3\text{-}CHRC_6H_5)$ (R = H, **3A**; R = OCH_3, **3B**) have been prepared and fully characterized spectroscopically. Only one ^1H NMR resonance was observed for the benzylic hydrogen of complex **3B**, indicating the presence of only the syn isomer (>98:2). The fluxional processes of **3A** and **3B** were studied by variable-temperature ^1H NMR. The rates of site exchange for the benzylic and ortho hydrogens of **3A** were the same, indicating that, in the intermediate 16e η^1-benzyl complex $Cp(CO)Fe(\eta^1\text{-}CH_2C_6H_5)$ (**2A**), aryl rotation and inversion of configuration at iron occur before collapse of **2A** to **3A**. Site exchange for the ortho hydrogens of **3B** was observed to occur with a barrier greater than that for ortho hydrogen exchange in **3A**. (i.e. 15.4 kcal/mol for **3B**, 12 kcal/mol for **3A**).

The rate of collapse of **2A** to **3A** was determined by an excited-state absorption experiment to be 1×10^8 s^{-1} ($\Delta G^{\ddagger}$ = 6.5 kcal/mol, T = 293 K). From this data the ground-state energy difference between **2A** and **3A** was calculated to be 5 kcal/mol, giving an equilibrium ratio of **2A** to **3A** of 1:10^4 at 293 K.[32]

The rates of trapping of **3A** and **3B** with PR_3 (R = Ph, Et) were determined by ^1H NMR. The $\Delta G^{\ddagger}$'s for trapping **3A** and **3B** with PPh_3 are 14.5 and 16.3 kcal/mol, respectively. This data coupled with the dynamic NMR and excited-state absorption data allowed the construction of a complete free energy diagram for the trapping of **3A** with PPh_3 (Figure 4). Likewise, from the data given here and in the preceding paper,[1] a free energy diagram giving a detailed kinetic and thermodynamic description of the formation of and PPh_3 dissociation from the two diastereomers of Cp-

$(CO)(PPh_3)FeCH(OCH_3)C_6H_5$ (**4**) was constructed (Figure 5). The results of the experiments presented herein and their kinetic and thermodynamic interpretations fully support and complement the synthetic and mechanistic analysis given in the preceding paper.

Experimental Section

All manipulations were performed under a nitrogen atmosphere by standard or modified Schlenk techniques unless otherwise noted. NMR spectra were recorded on an IBM AC-200 spectrometer. Probe temperatures were calibrated with the difference in ^1H chemical shifts of OH and CH_3 in a methanol standard. Infrared spectra were recorded on a Beckmann 4250 spectrophotometer with the polystyrene absorbance at 1601 cm^{-1} as reference. UV/visible spectra were recorded on a Hewlett-Packard Model 8415A spectrophotometer with 1-cm path length matched quartz cuvettes.

Toluene, benzene, and hexanes were rendered dry and oxygen-free by distillation from sodium/benzophenone under a nitrogen atmosphere. Toluene-d_8 was purchased from Aldrich, degassed by successive freeze/pump/thaw cycles, and stored under nitrogen. Ethyl acetate was degassed before use. PEt_3 was purchased from Strem and stored under nitrogen. PPh_3 was purchased from Aldrich and used as received. $Cp(CO)_2FeCH_2C_6H_5$[29] and $Cp(CO)_2FeCH(OCH_3)C_6H_5$[30] were prepared according to literature methods. Products $Cp(CO)(PPh_3)FeCH(OCH_3)C_6H_5$,[30] $Cp(CO)(PPh_3)FeCH_2C_6H_5$,[31] and $Cp(CO)(PEt_3)FeCH(OCH_3)C_6H_5$[1] are known compounds.

The apparatus used in the low-temperature photochemical reactions utilized a nitrogen boil-off system. Liquid nitrogen was boiled off through a vacuum-jacketed heavy-wall glass tube to cool a Schlenk tube filled with dry, degassed toluene. Sample solutions placed in 5-mm NMR tubes were immersed in the toluene-filled Schlenk tube, cooled to the desired temperature (temperature is monitored by a low-temperature thermometer immersed in the toluene solution), and photolyzed with a sunlamp (GE H100pf144-4 Reflector Flood Lamp).

Synthesis of $Cp(CO)Fe[\eta^3\text{-}CH(R')C_6H_5]$ Complexes [3A, R' = H; 3B, R' = OCH_3]. A total of 6–8 mg of $Cp(CO)_2FeCH(R')C_6H_5$ was dissolved in 500 μL of toluene-d_8, cooled to −80 °C (with the apparatus described above), purged with nitrogen, and photolyzed with a sunlamp for 20 min. The reaction mixture rapidly changes from clear yellow to dark red as the photolysis proceeds. Samples were removed for IR analysis at ambient temperature. The reaction mixture was kept at −78 °C prior to being placed in the NMR probe −78 °C. Spectroscopic data for the starting dicarbonyl complexes and η^3-benzyl products are summarized in Tables I and II. Although **3A** and **3B** were judged to be pure spectroscopically and could be warmed to above room temperature in a sealed NMR tube for a short time in solution, they could not be isolated as pure materials.

Determination of the Barrier to Collapse of 2A to 3A by an Excited-State Absorption Spectroscopy–Laser Kinetic Spectrophotometry Experiment. Excited-state absorption was performed in a single wavelength mode with the attenuated third harmonic output of a Quanta-Ray DCR-2(A)-10 Nd:YAG laser for excitation. The third harmonic output of the laser (355 nm) was isolated with a notch filter and attenuated with wedged reflectors to an incident energy level of 6.7 mJ/0.85-cm diameter at a repetition rate of 1 Hz. Excited-state absorption was monitored at a right angle to the excitation beam by a pulsed 150-W short-arc xenon lamp contained in a PRA LH215 housing and passed through 420-nm and IR cutoff filters. Lamp pulsing and electronic synchronization was controlled with circuits of our own design. An electromechanical shutter exposed the sample to the probe beam at the desired time, preventing unnecessary photolysis of the solution. The probe beam was collected with optics (f/4.5) and imaged on the slit of a Bausch & Lomb 0.5-m, f/4.4 single-grating monochromator set at 460 nm with a band-pass of 5 nm. The dispersed radiation was then softly focused onto the photocathode of a Hammamatsu R446 photomultiplier wired for five stages of gain and biased with an EMI-Gencom R-3000 HV power supply. The anode response (across a 50-Ω load) is linear at peak currents <9 mA. Base-line restoration of the photomultiplier's transient current was performed with an active analog backoff circuit of our own design and time-resolved with a Tektronix 7912AD transient digitizer (500-MHz bandwidth) interfaced with an IBM-PC microcomputer. The experiment measured the difference in absorption between the ground and excited states at 460 nm as a function of time.

A 1.3×10^{-4} M solution of **1A** ($Cp(CO)_2FeCH_2C_6H_5$; 3.5 mg in 100 mL of hexanes) was placed in a two-bulb (one for sample and one for waste) photolysis cell fitted with four optical-grade Pyrex windows. The sample was rigorously degassed by performing five successive freeze/pump/thaw cycles at pressures at or below 2×10^{-5} Torr and sealed under vacuum. The aliquot was shielded from extraneous light at all times during handling. Approximately 2-mL aliquots were exposed to the excitation beam while their absorbance differences at 460 nm were monitored. Kinetic traces of this change in absorbance were obtained by exchanging the aliquot with fresh solution for each cycle of the optical pump and probe and signal averaging results. The data presented here resulted from the averaging of 64 pump and probe cycles. Although no byproducts were detected in these experiments, at sufficiently high concentrations (ca. 10^{-3} M) an insoluble brown precipitate formed.

Trapping of $Cp(CO)Fe(\eta^3\text{-}CH(R')C_6H_5)$ Complexes (R' = H, OCH_3) with Phosphine Ligands PR_3 (R = Ph, Et). $Cp(CO)Fe(\eta^3\text{-}CH(OCH_3)C_6H_5)$ (**3B**) was generated at −80 °C as described above. A total of 1.1 equiv of PR_3 dissolved in 110 μL of toluene-d_8 was added to the η^3-benzyl solution at −80 °C. The sample was placed in the NMR probe at −78 °C and slowly warmed. The ^1H NMR spectrum remained unchanged until reaching −50 °C, and then signals for **3B** began to disappear and product signals grew in. When trapping was complete, the deep red color of **3B** had discharged, yielding a clear orange-yellow solution. The diastereomer ratios and spectral data for the products of trapping **3B** with PPh_3 and PEt_3 are summarized in Table IV. Rates of PR'_3 trapping were determined by ^1H NMR at −42 °C by integration, measuring the decrease of the $-OCH_3$ peak at δ 3.40 of **3B** versus residual $C_6D_5CD_2H$ at δ 2.09, which was used as an internal standard. Data are summarized in Table V. **3B** was trapped with a 200-μL toluene-d_8 solution containing the indicated number of equivalents of phosphine relative to **3B**. The reaction followed pseudo-first-order such that a plot of −ln [**3B**] versus time (seconds) gave the rate of phosphine trapping (see supplementary material for raw kinetic data and first-order plots).

$Cp(CO)Fe(\eta^3\text{-}CH_2C_6H_5)$ (**3A**) was generated at −80 °C as described above. A total of 1.1 equiv of PR'_3 dissolved in 110 μL of toluene-d_8 were added at −80 °C. The sample was placed in the NMR probe at −78 °C. PPh_3 trapping had already begun and was complete before the sample was warmed to −50 °C. PEt_3 trapping occurred before the sample, which was cooled to −80 °C, could be transferred into the NMR probe at −80 °C. Spectral data for products of trapping **3A** with PPh_3 and PEt_3 are summarized in Table IV. **3A** was trapped with a 200-μL toluene-d_8 solution containing the indicated number of equivalents of phosphine relative to **4**. The rate of phosphine trapping was determined by ^1H NMR at −71 °C for PPh_3 but could not be measured for PEt_3 because complete trapping occurred before the sample could be inserted into the NMR probe despite repeated attempts to keep samples cold. The rate was measured by integration, with the decrease of the η^5-C_5H_5 peak at δ 3.41 for **3A** versus residual $C_6D_5CD_2H$ at δ 2.09, which was used as an internal standard. The rate of PPh_3 trap is given in Table V and is derived from a plot of −ln [**3A**] versus time (seconds) (see supplementary material for raw kinetic data and first-order plots).

$(\eta^5\text{-}C_5H_5)(CO)(PEt_3)FeCH_2C_6H_5$. A total of 500 mg (1.87 mmol) of **1A** was dissolved in 50 mL of benzene in a Pyrex photolysis tube fitted with an ice-water-cooled cold finger. A total of 1.1 mL (7.47 mmol) of PEt_3 was added, and the solution was purged with nitrogen and photolyzed with a sunlamp. The starting clear yellow solution turned clear orange as the reaction progressed. The progress of the reaction was monitored by IR spectroscopy with the disappearance of absorption bands at 2000 and 1950 cm^{-1} for **1A** and appearance of a single absorption band for product at 1920 cm^{-1}. Solvent was removed in vacuo and the crude red product oil chromatographed on neutral alumina with 10:1 hexanes:ethyl acetate. The product eluted as a yellow band. Solvent removal in vacuo yielded 609 mg (91%) of orange powder as product. IR (C_6H_6): 1920 cm^{-1}. ^1H NMR ($C_6D_4CD_3$): δ 0.80 (dt, 9 H, J = 14.2, 7.4 Hz, $P\text{-}CH_2CH_3$), 1.19 (m, 6 H, $P\text{-}CH_2$), 1.70 (dd, 1 H, J = 8, 8 Hz, CHH'), 2.26 (dd, 1 H, J = 8, 5 Hz, CHH'), 3.65 (s, 5 H, η^5-C_5H_5), 7.06–7.37 (m, 5 H, C_6H_5). Anal. Calcd for $C_{19}H_{27}FePO$: C, 63.71; H, 7.55. Found: C, 63.48; H, 7.41.

Acknowledgment is made to the donors of the Petroleum Research Fund, administered by the American Chemical Society, and to the National Institutes of Health (Grant GM-23938) for the support of this research. We thank T. J. Meyer for advice

(29) Bibler, J. P.; Wojcicki, A. *J. Am. Chem. Soc.* **1966**, *88*, 4862.
(30) (a) Brookhart, M.; Nelson, G. O. *J. Am. Chem. Soc.* **1977**, *99*, 6099. (b) Brookhart, M.; Studabaker, W. B.; Humphrey, M. B.; Husk, G. R. *Organometallics*, in press.
(31) Stanley, K.; Baird, M. C. *J. Am. Chem. Soc.* **1975**, *97*, 4292.
(32) **Note Added In Proof.** Herrick, R. S.; Frederick, A. B.; Duff, R. R., submitted for publication in *Organometallics*. They have measured the rate of trapping **3A** by CO. Their results indicate that the transient, which decays with $t_{1/2} \sim 60$ ns, is not due to trapping **3A** by CO. Thus, the results shown in Figure 2 support *two* isomerization processes, possibly decay of **2A** to carbene hydride ($t_{1/2} \sim 7$ ns), which in turn is converted to **3A** via **2A** ($t_{1/2} \sim 60$ ns). The calculated equilibrium ratio **2A**:**3A** is not significantly altered (Figure 3).

and use of the laser flash apparatus and R. S. Herrick for communication of unpublished results.

Registry No. 1A, 12093-91-3; **1B**, 64494-50-4; **2A**, 117098-27-8; **2B**, 117098-28-9; **3A**, 117098-24-5; **3B**, 117098-25-6; (*SR*):(*RS*)-**4**, 104832-41-9; (*RR*):(*SS*)-**4**, 113350-82-6; (*SR*):(*RS*)-**5**, 113215-01-3; (*RR*):(*SS*)-**5**, 113109-99-2; **8**, 33135-99-8; **9**, 117098-26-7.

Supplementary Material Available: Kinetic data and plots for trapping **3B** with $P(C_2H_5)_3$ and $P(C_6H_5)_3$ and **3A** with $P(C_6H_5)_3$ and UV/vis spectrum of **1A** (10 pages). Ordering information is given on any current masthead page.

Hexaisopropoxyditungsten and Dodecaisopropoxytetratungsten: $W_2(O\text{-}i\text{-}Pr)_6$ and $W_4(O\text{-}i\text{-}Pr)_{12}$. 2.[1] Studies of Cluster Dynamics and the Equilibrium between the 12-Electron Cluster and Two Metal–Metal Triple Bonds. A Symmetry-Allowed $[\pi^2_s + \pi^2_s]$ Cycloaddition Reaction and Comparisons with the Chemistry of Cyclobutadiene[2]

Malcolm H. Chisholm,* David L. Clark, and Mark J. Hampden-Smith

Contribution from the Department of Chemistry, Indiana University, Bloomington, Indiana 47405. *Received March 21, 1988*

Abstract: In toluene-d_8, the C_{2h}-rhomboidal 12-electron cluster $W_4(O\text{-}i\text{-}Pr)_{12}$ is shown to undergo a dynamic process on the NMR time scale, E_{Act} ca. 15 kcal mol^{-1}, in which the W–W double and single bonds migrate around the W_4 ring. A symmetrical rhombus, D_{2h}-$W_4(\mu\text{-}O)_4(O)_8$, is the transient structure. This motion of the metal atoms is coupled with a *correlated rotation* [Mislow, K. *Acc. Chem. Res.* **1976**, *9*, 26] about the W–O bonds of the O-*i*-Pr ligands attached to the wingtip W atoms such that proximal and distal W–O-*i*-Pr group exchange occurs. The combined motions are called the *Bloomington Shuffle* and do not involve the backbone W atoms and their attendant O-*i*-Pr ligands. A square, D_{4h}-$W_4(\mu\text{-}O)_4(O)_8$ transition state is not involved. The *Bloomington Shuffle* and the equilibrium between $W_4(O\text{-}i\text{-}Pr)_{12}$ and $2W_2(O\text{-}i\text{-}Pr)_6$ bring about a metathesis of the tungsten atoms of the W≡W bond in $W_2(O\text{-}i\text{-}Pr)_6$. The equilibrium $W_4(O\text{-}i\text{-}Pr)_{12} = 2W_2(O\text{-}i\text{-}Pr)_6$ has been studied as a function of temperature (23 to +44 °C) leading to a determination of the thermodynamic parameters $\Delta H° = +21$ (2) kcal mol^{-1} and $\Delta S° = +61$ (6) eu. The approach to equilibrium in toluene-d_8 has also been studied as a function of six temperatures in the range +23 to +44 °C starting from both $W_4(O\text{-}i\text{-}Pr)_{12}$ and $W_2(O\text{-}i\text{-}Pr)_6$. Analyses of the kinetic data reveal the activation parameters (i) for $W_4 \rightarrow 2W_2$, $\Delta H^‡ = +30$ (2) kcal mol^{-1} and $\Delta S^‡ = +18$ (6) eu, and (ii) for $2W_2 \rightarrow W_4$, $\Delta H^‡ = +10$ (1) kcal mol^{-1} and $\Delta S^‡ = -39$ (3) eu. In the coupling of two $W_2(O\text{-}i\text{-}Pr)_6$ units there is a highly ordered transition state and these results are compared to organic cycloaddition reactions. A molecular orbital analysis for the cycloreversion reaction $W_4(O\text{-}i\text{-}Pr)_{12} \rightarrow 2W_2(O\text{-}i\text{-}Pr)_6$ along a C_{2h} reaction path has been developed with the Fenske–Hall calculational method. A Walsh diagram has been constructed and an analysis of avoided crossings, real and trivial, is presented. The system is closely compared to the coupling of two ethyne molecules to give cyclobutadiene. While the latter is a symmetry-forbidden $[\pi^2_s + \pi^2_s]$ reaction in the Woodward–Hoffmann sense, the coupling of two $W_2(OH)_6$ molecules to give C_{2h}-$W_4(OH)_{12}$ is shown to be symmetry allowed.

In the previous paper[1] we described the synthesis of the first example of a metal–metal multiply bonded compound $W_2(O\text{-}i\text{-}Pr)_6(M{\equiv}M)$ and its dimer, a tetranuclear 12-electron cluster, $W_4(O\text{-}i\text{-}Pr)_{12}$. We were fortunate in obtaining a crystalline sample that contained a 1:1 mixture of the dinuclear and tetranuclear molecules in the unit cell while independent synthetic routes to each compound were established. The dinuclear compound is a member of a now extensive series of ethane-like $X_3M{\equiv}MX_3$ compounds.[3] The tetranuclear compound adopts a centrosymmetric structure in the solid state involving a central $W_4(\mu\text{-}O)_4(O)_8$ unit with virtual C_{2h} symmetry. The M_4 unit is a distorted rhombus with two short, 2.50 (1) Å, and two long, 2.73 (1) Å, M–M distances corresponding formally to W–W double and single bond distances, respectively. The preference for a distorted rhombus of metal atoms relative to a symmetrical square, D_{4h}, or rhombus, D_{2h}, having equal M–M distances, was explained as a result of a 2nd order Jahn–Teller effect. Indeed calculations on the symmetrical D_{4h} $W_4(\mu\text{-}OH)_4(OH)_8$ model compound indicate a direct analogy with cyclobutadiene.[4] In the D_{4h} (square) structure both compounds (C_4H_4 and $W_4(O\text{-}i\text{-}Pr)_{12}$) give rise to a diradical ground state. In this paper we describe our studies of the dynamic behavior of the cluster and the equilibrium, eq 1. Fascinating similarities and differences are again seen in comparing the chemistry of the M≡M and C≡C bonds of configuration $\sigma^2\pi^4$ and their 12 electron clusters.

$$W_4(O\text{-}i\text{-}Pr)_{12} \underset{k_{-1}}{\overset{k_1}{\rightleftharpoons}} 2W_2(O\text{-}i\text{-}Pr)_6 \qquad (1)$$

Results and Discussion

Cluster Dynamics. The Bloomington Shuffle. The solid-state structure of the central core of $W_4(O\text{-}i\text{-}Pr)_{12}$ is represented diagramatically in Figure 1 [where arrows at the oxygen atoms are used to define the orientation of the methine vectors]. We believe that the gross features of this structure are maintained

(1) Part 1: Chisholm, M. H.; Clark, D. L.; Folting, K.; Huffman, J. C.; Hampden-Smith, M. J. *J. Am. Chem. Soc.* **1987**, *109*, 7750.
(2) Dedicated to Professor Kurt Mislow on his retirement.
(3) Chisholm, M. H. *Angew. Chem., Intl. Ed. Engl.* **1986**, *25*, 11.
(4) For a discussion of the bonding and dynamic behavior of neutral C_4H_4 see: Davidson, E. R.; Borden, W. T. *J. Chem. Phys.* **1983**, *87*, 4783; *J. Am. Chem. Soc.* **1978**, *100*, 388; *Acc. Chem. Res.* **1981**, *14*, 69.

0002-7863/89/1511-0574$01.50/0